1
Current Concepts for Optical Path Enhancement in Solar Cells

Alexander N. Sprafke and Ralf B. Wehrspohn

1.1
Introduction

The conversion efficiency of a solar cell, that is, the ratio of electrical power extracted from the cell to the power of solar photons flowing into the cell, is directly connected to the number of photons absorbed in the absorber material of the cell. Therefore, it is of critical importance to insert as many photons as possible into the cell and keep them inside the cell until they are finally absorbed. While achieving the first aspect is referred to as antireflection, the second aspect is commonly called optical path enhancement, also known as light Trapping, which is the focus of this chapter.

Because of its fundamental significance to the solar-to-electrical conversion mechanism, light trapping should be considered for any solar absorber material. However, light trapping is of particular importance for solar cells based on crystalline silicon (c-Si). Owing to its abundance and to the long-existing mature technologies in the electronic industry, commercial c-Si based solar cells are widely available and dominate the PV market today [1]. But since c-Si is an indirect semiconductor, it is actually a relatively bad light absorber. Figure 1.1 shows the absorption depth δ of c-Si. λ of an absorbing material is defined as the distance at which the intensity of light decreases to $1/e$ after it enters the material. For wavelengths $\lambda < 500$ nm, most of the light energy is absorbed within a micron. For longer wavelengths, λ increases rapidly (note the logarithmic y-axis) and reaches values in the range of centimeters for wavelengths in the spectral range of the bandgap of c-Si at around $\lambda \approx 1150$ nm.

To compensate for this, one could either use thick c-Si absorbers, or apply light-trapping schemes to optically thicken the absorber material. Owing to high costs and challenging requirements on material quality, using millimeter or centimeter thick c-Si absorbers is not an option. In fact, quite contrary is the case. The current trend in the PV industry as well as in the research community is to develop concepts to increase material efficiency by decreasing the Si wafers thickness below 100 μm. To stay competitive, the conversion efficiency of thin c-Si cells needs to be

Photon Management in Solar Cells, First Edition. Edited by Ralf B. Wehrspohn, Uwe Rau, and Andreas Gombert.

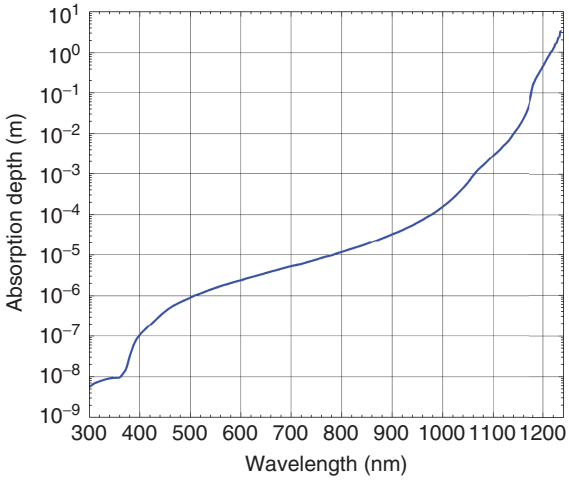

Figure 1.1 Absorption depth λ of crystalline silicon plotted against the wavelength λ of light. The optical properties to calculate λ were taken from Ref. [2].

higher or at least comparable to the efficiency of 180 µm thick, commercial solar cells available today.

In Figure 1.2 calculated absorption spectra of bare planar c-Si slabs of different thicknesses d are plotted. From the absorption at small wavelengths one can easily see that independent of the thickness light incoupling into silicon is rather weak despite the very high absorption coefficient of silicon in this spectral range (compare Figure 1.1). This is due to the strong refractive index contrast between silicon and air of $n_{\mathrm{Si}}/n_{\mathrm{air}} \approx 3,5$ in the visible spectral region and could be overcome by applying means of antireflection. Much more severe in the context of photovoltaic applications is the strong loss of absorption when decreasing the thickness of the c-Si slab. For a thickness of $d = 200$ µm, a typical thickness for commercially available c-Si solar cells, there is considerable absorption up to $\lambda \approx 950$ nm which then starts to decrease toward the spectral position of the band edge of c-Si. Thinning the c-Si slab leads to a drastic reduction of absorption and shifts the absorption edge to shorter wavelengths. For example, the integrated absorption for the $d = 0.5$ µm and the $d = 10$ µm slab is only 7.8% and 69% of that of the 200 µm slab, respectively (integrated from $\lambda = 400$ nm to 1200 nm).

These examples underly the importance that effective concepts for optical path length enhancement are inevitable for future solar cell designs. Here, we chose c-Si as an example material; however, in principle, these considerations apply to any solar cell material and have to be taken into account.

1.2
Planar Antireflection Coatings

From an optics point of view, the simplest solar cell consists of an homogeneous slab as introduced in the previous section, with an optical thickness of

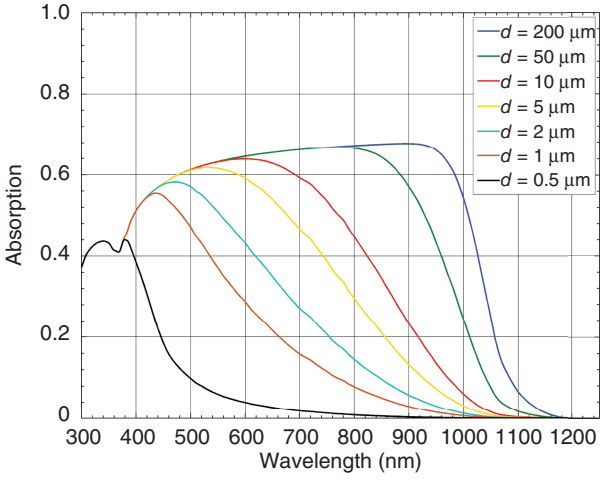

Figure 1.2 Calculated absorption spectra of planar c-Si slabs of varying thickness d suspended in air at normal light incidence. Note, that since the coherence length of sunlight is < 1 µm, incoherent light was assumed in the calculations.

$d_{\text{opt}} = nd/\cos\theta_2$, where n and d are the refractive index and the geometrical thickness of the cell, respectively, and θ_2 is the angle of refraction (see Figure 1.3a for illustration). As pointed out above, a rather large amount of light energy does not reach the absorbing region but is reflected at the top surface. For example, the reflectivity of bare silicon is $R \approx 35\%$ for a wavelength of $\lambda = 600$ nm and normal incidence (compare Figure 1.2). Coupling a greater amount of light energy into the cell is commonly achieved by applying a planar antireflection coating (ARC) on top of the cell. This coating consists of a dielectric layer with a thickness of $\lambda/4$ such that the light wave reflected from the top surface and the wave reflected from the dielectric–semiconductor interface interfere destructively resulting in $R = 0$ in an ideal case for a particular design wavelength λ_{des}. In commercial photovoltaic applications mostly SiN deposited by chemical vapor deposition is applied as a coating material. A thickness of $d \approx 70$ nm minimizes reflection at $\lambda_{\text{des}} = 600$ nm, which is close to the peak of the solar spectrum and is responsible for the commonly known dark-bluish appearance of commercially available c-Si solar cells. A single-layer ARC minimizes light reflection of a particular design wavelength and angle of incidence only. This is in conflict with the broad solar spectrum and to the ever-changing altitude of the sun during the day. It is possible to minimize reflection losses for more than one wavelength by the use of double- or even more complex multi-layer antireflection coatings. However, another conceptual disadvantage of planar interference-based ARCs is their inherent symmetric mode of operation: They increase the flow of incoming light into the cell (at least for the design wavelength). However, photons that are not absorbed during their first pass through the cell and eventually reach the interface of the ARC again because of a scattering event or reflection at a mirror at the backside, are now efficiently coupled out of the solar cell. Thus, an ARC does not offer

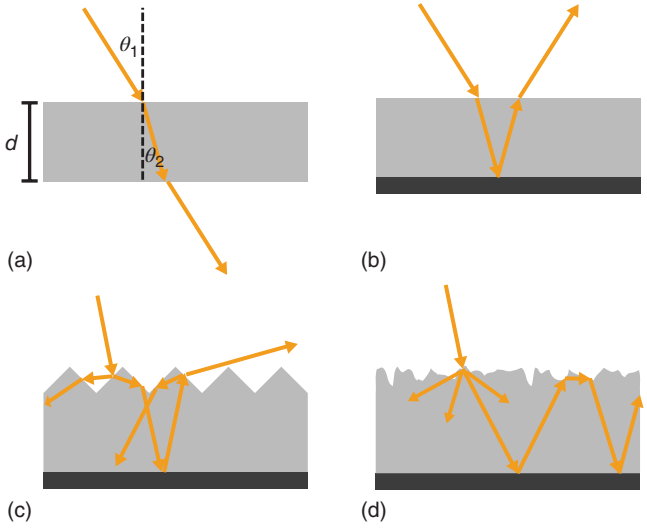

Figure 1.3 Light trapping concepts: (a) bare, planar slab of the absorber material, no light trapping applied, (b) backside reflector, (c) pyramidal texture, (d) random scattering texture. Sketched structures are not to scale.

any light trapping and additional or completely different concepts need to be considered to accomplish sufficient optical light path enhancement.

1.3 Optical Path Enhancement in the Ray Optical Limit

Light trapping in commercially available c-Si solar cells utilizes approaches that are based on ray optics. The most simple tool in this context would be a mirror at the backside of the absorber, which leads to a doubling of the optical light path (see Figure 1.3b); thus, the optical path enhancement is $\alpha_{opt} = 2$. A common approach to achieve real light trapping is to change the propagation direction of the light such that total internal reflection occurs (for a silicon–air interface, the critical angle is $\theta_c \approx 16°$). To achieve internal light trapping one has to move from planar surfaces to textured surfaces.

The frontside of commercial c-Si based solar cells are textured by alkaline or acidic chemical wet-etching [3, 4]. For example, anisotropic alkaline wet-etching of monocrystalline material (the <100> orientation is preferentially etched) results in randomly arranged pyramidal structures with feature sizes in the $\approx 10\,\mu m$ range. Using lithographic steps for inverted pyramids are also possible. In these structures light reflected from the surface gets a second chance to enter the absorber because of the tilted surfaces of the pyramids thereby leading to less reflection back into the upper halfspace (see Figure 1.3c). Additional ARCs may further decrease the reflection of the textured surface. Since the frontside is not

planar anymore, light will be coupled into the silicon obliquely, not only leading to some optical path length enhancement, but also enabling total internal reflection for light rays coming back to the frontside. Thus, true optical path length enhancement is achieved. Today's world record single-junction silicon solar cell, the PERL cell [5] with a conversion efficiency of more than 24%, which uses pyramidal surface structures, holds the current world record as the single-junction silicon solar cell. In this case, inverted pyramids are arranged in a square lattice pattern (lattice constant ≈ 20 µm). To obtain high-efficiency c-Si solar cells with pyramidal front side textures one has to carefully optimize the geometric parameters of the pyramids to match the actual wafer thickness. Otherwise, light can be effectively coupled out of the cell because a large fraction of back-reflected light hits the pyramidal facets perpendicularly [3]. In solar cells based on materials that do not offer an easy way to obtain pyramidal structures , for example, thin GaAs membranes, texturing may be introduced in additional layers such as structured coatings [6].

1.4 Scattering Structures for Optical Path Enhancement

A very effective light trapping concept is the full randomization of the propagation directions of the incident sunlight after hitting the first absorber interface. A Lambertian scatterer at the front surface of the absorber material offers the highest degree of randomization [7]. In this case, the incoming light is scattered into propagation directions with a cosine distribution. The optically thicker medium, which is usually the absorber material, offers a larger phase space for light to be filled than does the adjacent medium (e.g., air). Thus, light will be preferably scattered into the absorber instead of out of it leading to a high confinement of light inside the desired volume. Additionally, an ideal Lambertian scatterer operates independently of the angle of incidence. This scenario was first elaborated by Eli Yablonovitch in 1982 [7]. He found the upper limit of light path enhancement for random scattering textures to be $\alpha_{opt} = 4n^2$, where n is the refractive index of the solar cell. For this limit, nowadays commonly referred to as the Yablonovitch or Lambertian limit, illumination from the frontside, a Lambertian front side texture and a perfect mirror at the backside are assumed (Figure 1.3d). Yablonovitch's theory applies in the limit of vanishing absorption, but has been generalized to apply for arbitrary absorption by Green [8]. For example, for a solar cell made of silicon $\alpha_{opt} \approx 50$ is theoretically possible.

A particularly interesting example of a material class that exhibits strong diffuse scattering close to the Lambertian case is *black silicon* (b-Si) [9–11]. Black Si surface textures consist of densely packed needle-like peaks and pits of irregular shape and high aspect ratios (see Figure 1.4(a)). Black silicon can be prepared by several methods such as metal-assisted wet-chemical etching, inductively coupled reactive ion etching (ICP-RIE), or short-pulse laser irradiation [11–15]. Another important advantage of b-Si over conventional pyramidal textures is the comparatively large feature sizes of the latter. Application of pyramidal textures will fail

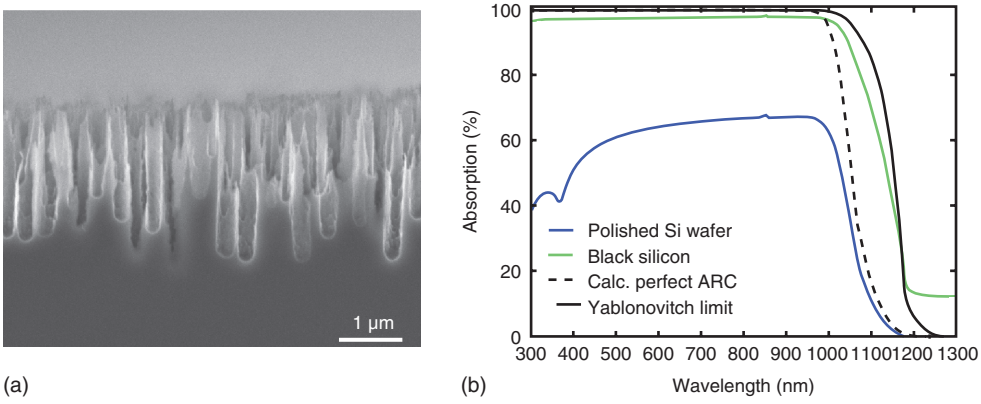

Figure 1.4 (a) SEM cross section of a typical b-Si sample fabricated by ICP-RIE. (b) Experimental absorption spectra of a b-Si structure (green line). For comparison the measured absorption spectra of a polished Si wafer (solid blue) as well as theoretical spectra of a perfect ARC (dashed black) and a perfect ARC with Lambertian scattering (Yablonovitch limit, solid black) are also plotted (adapted from Ref. [14]).

when the wafer thickness comes to values below 50 µm. For such thin wafers, b-Si is a suitable alternative.

A typical experimentally measured absorption spectrum of b-Si prepared by ICP-RIE is plotted in Figure 1.4(b) next to the spectrum of a bare c-Si wafer and calculated spectra of a wafer for which an ideal ARC but no light trapping is assumed, and the Yablonovitch limit, that is, with maximum light trapping. The b-Si sample reveals an almost complete suppression of the reflectivity over a broad spectral range making it far more effective than conventional ARCs. In the spectral region of the band gap of silicon, b-Si clearly outperforms a theoretical perfect ARC, which has to be attributed to its excellent light trapping properties. The absorption in the spectral region of the bandgap is very close to the Yablonovitch limit (see also Figure 1.10). The extraordinary antireflection and light trapping features of b-Si may be explained by an intuitive picture: On the one hand, the top of the texture consists of frayed tips of deep sub-wavelength dimensions that broaden slowly toward the wafer. Therefore, the surface can be treated as an effective medium with a smooth varying refractive index resulting in negligible back reflection, even for quasi-omnidirectional light incidence [16, 17]. On the other hand, the feature sizes at the bottom of the structure are in the range of a few hundred nanometers, that is, have dimensions of the wavelength of the incoming light. Thus, the bottom parts of the texture act as very effective light scatterers resulting in efficient randomization which is a condition for Lambertian light trapping. This makes black silicon an ideal candidate for photovoltaic applications, especially for ultrathin devices with a thickness below 50 µm.

Solar cell prototypes made of b-Si have already been demonstrated with efficiencies of up to 18.7% [11, 13, 18–21]. However, due to its strongly enlarged surface

area and defect density, b-Si exhibits rather poor electronic surface quality, that is, high electronic recombination losses and degradation effects, which strongly affect solar cell device performance especially at short wavelengths [22, 23]. Nevertheless, it has been shown recently that an appropriate passivation of the b-Si surface by a conformally deposited Al_2O_3 layer can effectively compensate for these effects [14].

A thorough review on b-Si for photovoltaics will be given in Chapter 5 [24]. This section has also not covered scattering structures for thin-film photovoltaics such as amorphous and microcrystalline solar cells. These are treated in Chapter 4.

1.5
Resonant Structures for Optical Path Enhancement

Taking the simple planar slab model of the solar cell as introduced in Figure 1.3a, the maximum optical path enhancement is obviously attained when the impinging light is redirected to propagate parallel to the boundaries. In the case of normal light incidence this would mean a directional change of 90°.

Structures that are able to accomplish such a rather large redirection of the optical path are diffractive elements, such as gratings. A possible light path involving a diffraction grating in a solar cell may be described as sketched in Figure 1.5. Sunlight enters the absorber material of the cell. A reflection grating placed at the backside of the cell diffracts the light into at least one diffraction order m other than the 0th order as long as the grating constant is larger than the considered wavelength of light (for normal incidence). The amount of light energy going into a specific diffraction order is given by the diffraction efficiency, which crucially depends on the precise geometry of the actual grating [25]. Only light of a particular wavelength λ_g will be diffracted into a grazing angle as demanded, that is, into a direction parallel to the boundaries (also known as Rayleigh anomaly [26]). For $\lambda < \lambda_g$ the diffracted light travels back to the front surface but with a much larger angle of incidence compared to light that would have been reflected by a simple

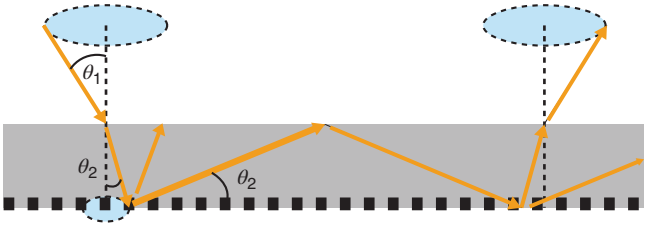

Figure 1.5 Possible light path inside a solar cell with a backside grating. After entering the cell the light is diffracted by a grating at the backside of the cell. Due to the shallow angle of the diffraction order total internal reflection is possible. Upon the second diffraction the light is possibly diffracted into the direction of the former 0th diffraction order and leaves the cell (adapted from Ref. [27]).

backside mirror. Thus, total internal reflection at the front side is enabled. Hereafter, the light is redirected back onto the grating structure and is diffracted again. Because of the reciprocity theorem the light now may be either diffracted into the direction of the former 0th diffraction order and thus eventually leave the cell, or it may be diffracted into a diffraction order which is again trapped in the cell by total internal reflection. Again, the redistribution ratios of the light energy into the different diffraction orders are determined by the precise diffraction efficiencies. Also, because of the different angle of incidence onto the grating in the second pass through the cell, additional diffraction channels may be possible, which may lead to further light trapping by total internal reflection.

For a more detailed analysis instead of considering perfectly collimated light the divergence angle of the sunlight $\Theta_S = 4.7$ mrad, or the even more realistic angular divergence of the circumsolar radiation $\Theta_C = 44$ mrad, must not be ignored. Then, the conservation of étendue has to be taken into account. Assuming that light rays impinging on the grating structure perpendicularly will experience a change of propagation direction of 90° and that every other ray, which has a slightly oblique incidence due to the angular divergence, follows the conservation of étendue, the maximum optical path length enhancement is found to be

$$\alpha_{opt} \approx \frac{2n\Theta}{1 - \cos\Theta} \tag{1.1}$$

for $\Theta << 1$ as derived in Ref. [27]. In case of silicon, this gives an enhancement factor of $\alpha_{opt} = 2980$ and $\alpha_{opt} = 318$ considering Θ_S and Θ_C, respectively. Strictly speaking, these results hold for rotational symmetry of the problem and unity diffraction efficiency for all wavelengths and angles of incidence only. Thus, this approach constitutes a theoretical upper limit for any diffraction-based structure and emphasizes the high potential to effectively trap light. To obtain realistic characteristics of grating structures integrated into solar cells, rigorous numerical calculations that take the wave nature of light fully into account, such as the finite-difference time-domain method [28], have to be conducted.

On the downside it has to be noted that the spectral width of diffractive elements might be too narrow for certain applications. This especially accounts for 2D gratings. Therefore, more complex 2D gratings have been suggested that exhibit a broader spectral response, but these structures suffer from lower maximum path enhancements [29]. Since diffraction-based light trapping concepts rely on the coupling of light into modes that are bound to the absorber material by total internal reflection, the ultimate lower limit for the absorber film thickness is dictated by the monomodal regime. An approach suggested by Yu *et al.* [29] to circumvent this situation is to decouple the active layer from the light-guiding layer.

Several concepts are discussed in the literature to realize resonant structures for light trapping including dielectric structures [30–32] as well as metallic structures such as metallic gratings and metal nanoparticle arrays, which additionally exploit plasmonic effects [33, 34]. Early works were performed by Morf and coworkers [31] who applied binary gratings to the backside of a solar cell. In particular, blazed

gratings are of interest since they exhibit enhanced diffraction efficiencies for certain diffraction orders in comparison to symmetric gratings. Morf and coworkers report path length enhancements of about $\alpha_{opt} \approx 5$ in these structures. The enhancement factor was determined by the change in reflectance which is a rather imprecise measure. An improved determination of the enhancement factor is to measure the spectrally resolved external quantum efficiency (EQE) enhancement

$$\alpha_{EQE}(\lambda) = \frac{EQE_w(\lambda)}{EQE_{w/o}(\lambda)}, \tag{1.2}$$

where the subscripts w and w/o indicate the EQE with and without the enhancing structure, respectively. It should be noted that in the limit of low absorption $\alpha_{EQE} = \alpha_{opt}$ holds. The first work using $\alpha_{EQE}(\lambda)$ as a measure was conducted by Zaidi *et al.* [35]. They found an enhancement factor of $\alpha_{EQE}(\lambda) = 2.7$ for a rectangular grating at the backside of a c-Si solar cell in the spectral region of low absorption at the band gap. Measurements on amorphous silicon–based solar cells revealed similar results [36]. Kimerling and coworkers investigated the combination of a grating and a dielectric Bragg mirror at the backside [37, 38]. They obtained $\alpha_{EQE}(\lambda) = 7$ and $\alpha_{EQE}(\lambda) = 135$ for a wavelength of $\lambda = 1100$ nm and $\lambda = 1200$ nm, respectively.

A systematic theoretical comparison of gratings, the combination of gratings with distributed Bragg reflectors (DBR), and 3D photonic crystals was conducted by the group of Joannopoulos [32]. 3D photonic crystal structures combine the properties of a grating (diffraction) and a mirror (reflection) and hence may reveal a similar or possibly higher potential. Joannopoulos *et al.* found that the efficiency of a 2 μm silicon solar cell can be increased by 25% by adding an optimized 1D grating to a DBR, 31.3% by a 2D grating instead of a 1D grating, and 26.3% by replacing the DBR with 2D photonic crystal. Using a 3D photonic crystal instead of any of these structures resulted in a slightly better enhancement of 26.5%.

Experiments using 3D photonic crystals on the backside of a silicon solar cell have been carried out very rarely. For example, in [39] it was found, that the short circuit current of a thin (1.5 μm) crystalline solar cell could be enhanced by 10% with a 3D photonic crystal on the backside in comparison to a reference cell without the crystal. The challenge is not only to create high-quality 3D photonic crystals such as inverted opals with a photonic band gap in the spectral range of the band gap of silicon, but also to transfer them to and integrate them into the solar cell.

Up to now the achieved optical path enhancements are still far from the limit given by the conservation of étendue (up to $\alpha_{opt} = 2980$ for silicon). Therefore, there is still a lot of room for more research on gratings and photonic crystals for light trapping in solar cells. A thorough review on the theory and technological realization of diffractive grating structures are given in Chapter 3.

An application field of photonic crystals that emerged during the recent years is that of integral photon management. Here, the absorber itself is structured as a 1D, 2D, or 3D photonic crystal which is very different from the approaches given above that leave the absorber material unaffected. This gives way to the exploitation of

effects not considered before for light trapping, for example, slow light phenomena to increase the interaction duration with the absorber material, manipulating light propagation at particular frequency ranges and into certain propagation directions [40–42]. This may shed new light on the well-known properties of photonic crystals.

1.6 Ultra-Light Trapping

As pointed out in the previous section, the sunlight illuminates the solar cell with a very small divergence Θ_S; the circumsolar radiation divergence Θ_C is just a little bit larger. At the same time light is able to escape from the cell into the entire half-space above the cell, that is, the angular escape cone is $\Theta_e = 2\pi$. The difference of the small cone of incidence and the large escape cone constitutes an avoidable loss mechanism. Because of light path reversibility the acceptance cone and the escape cone are essentially equal. Therefore, shrinking the acceptance cone to match the angular divergence of the incoming irradiation from the sun would also lead to a restriction of the escape cone to a much smaller value. A concept to narrow down the acceptance/escape cone is the use of angular-selective reflectance filters and implementation of a photonic light trap [27, 43].

Figure 1.6 sketches the working principle of this approach. Sunlight passes through an angular selective filter that features high transmittance for an acceptance cone matched to the angular divergence of the sun light and low transmittance but high reflectance for all other angles of incidence. Then, the light enters the absorbing region of the solar cell that is equipped with a scattering light trapping mechanism at the frontside. While part of the isotropically scattered light is trapped by total internal reflection, the residual light escapes from the active region into the space above to hit the angular selective filter again. Only light that is scattered into the small acceptance range of the filter is able to leave the system. All other light is reflected back into the active region of the cell. Because of the small acceptance range of the filter a tracking system which follows the course of the sun is necessary. In combination with this tracking system this concept is called ultra-light trapping.

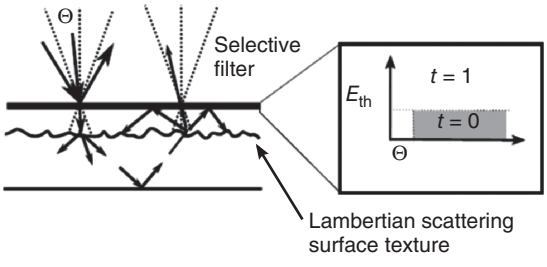

Figure 1.6 Schematic representation of the ultra-light trapping concept. Inset: Spectral range of an ideal angular selective filter (adapted from Ref. [43]).

In an ideal case, the angular-selective filter has unity transmittance for an angle of incidence smaller than the desired acceptance cone and unity reflectance for larger angles. Placed above a solar cell with a Lambertian-scatterering frontside and a perfect mirror at the backside, the maximal possible path length enhancement of this system is given by Goetzberger [44], Minano [45]

$$\alpha_{\text{opt}} = \frac{4n^2}{\sin^2\Theta}. \tag{1.3}$$

Inserting Θ_C results in a very large factor of optical path length enhancement of $\alpha_{\text{opt}} \approx 26 \times 10^3$ for silicon; inserting Θ_S even leads to $\alpha_{\text{opt}} \approx 2 \times 10^6$. The same values are derived for approaches involving concentration optics following the conservation of étendue. Additionally, for ultra-light trapping also the Shockley–Queisser limit for concentrating systems holds [46]. Ultra-light trapping and light concentration share a deep analogy to each other. This analogy is based on the fact that both concepts change the angular range of the acceptance cone. While the ultra-light trapping concept narrows down the acceptance cone to match the angular divergence of the sunlight, concentration systems work vice versa, that is, the angular divergence of the sunlight is enlarged to match the acceptance cone of the cell [47].

Until now, no experimental realization of ultra-light trapping has been conducted successfully to increase the efficiency of a solar cell. This is due to the fact that very few filters exist that exhibit the desired characteristics. Nevertheless, promising attempts have been conducted by Höhn *et al.* [48]. A comprehensive overview on the effects of different angular selective structures on silicon solar cells has been given by Ulbrich *et al.* [43, 49] and is also described in Chapter 7 of this book.

In addition to ideal filters, manufacturable rugate stacks and 3D photonic crystals were investigated in their work [43]. Rugate stacks show suppressed ripple formation in their optical spectra and no harmonic reflections as compared to Bragg stacks [50]. Iso-frequency surfaces for a frequency in the spectral region of the band gap of silicon are plotted in Figure 1.7(a) and (b) for a rugate filter and an inverted opal in Γ–X direction, respectively. Readers who are not familiar with this kind of plot may note that k_x,k_y, and k_z give the direction of the light impinging on the structure whereas the surface basically stands for available photonic states, that is, light of directions that are part of the surface will be able to enter the structure, otherwise it will be reflected. The acceptance cone of the rugate filter is given by the second photonic band (Figure 1.7(a)). The photonic density of states vanishes for increasing angles because the stop gap shifts to higher frequencies; thus, light impinging from outside the acceptance cone is reflected. This holds true until for even higher angles the lower edge of the stop gap reaches the frequency that is being plotted, that is, light is transmitted by the first band and more importantly light can escape from the device into these directions. For the 3D photonic crystal the inverted opal structure was chosen due to its well-known properties. On first sight it seems feasible to use the inverted opal in the Γ – L direction with the stop gap pointing to the sun and using the spectral shift of the

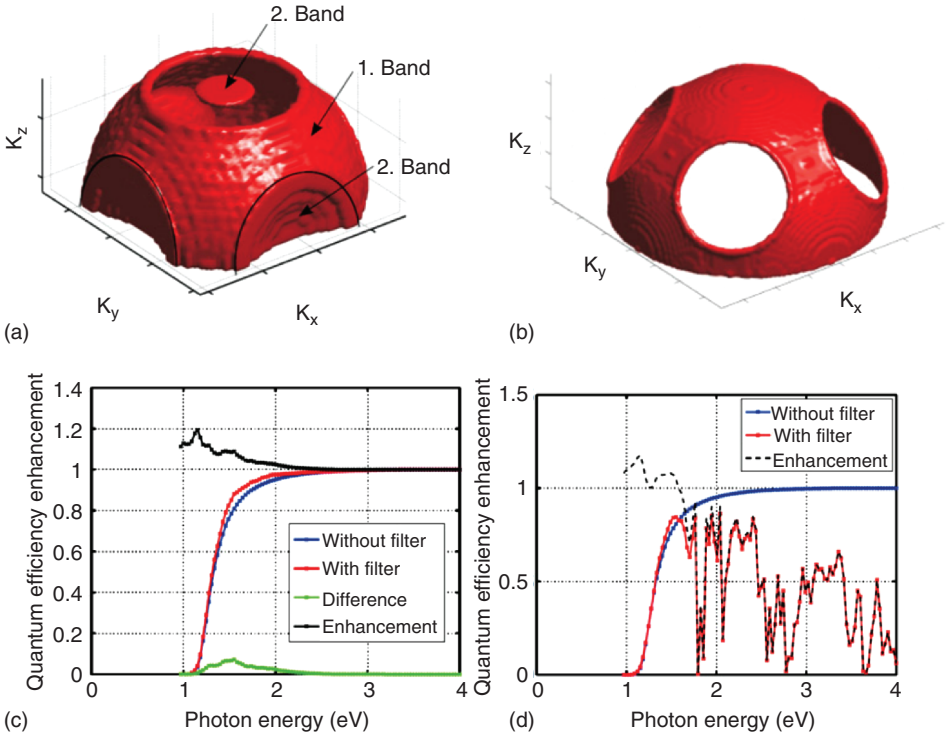

Figure 1.7 3D isofrequency surfaces of a rugate filter (a) and an inverted opal in $\Gamma - X$ direction (b). (c): Calculated quantum efficiency for an inverted opal grown in $\Gamma - X$ direction on top of a silicon solar cell. For photon energies above the photonic stop gap unity transmission is assumed. (d): Same as (c) but with realistic transmission properties (adapted from Ref. [43]).

stop gap similar to the mechanism of the rugate filter [51]. But it turns out that the use of the inverted opal in $\Gamma - L$ direction results in unwanted strong reflections from higher-order stop gaps. Using the inverted opal in $\Gamma - X$ direction enables to assign the stop gap itself for ultra-light trapping instead of the spectral shift of the stop gap. Figure 1.7(b) shows that the inverted opal in $\Gamma - X$ direction does not match its acceptance cone to that of the angular divergence of the sun as tight as the rugate filter, but it apparently reflects a larger fraction of the hemisphere back.

Assuming perfect transmission of the entire solar spectrum through an inverted opal in $\Gamma - X$ direction the calculated spectrally resolved quantum efficiency for a thin-film silicon solar cell is shown in Figure 1.7(c) [43]. Near the band gap of amorphous silicon the effect of the ultra-light trapping is visible. However, when the realistic transmission of the inverted opal is included, the efficiency of the device is clearly decreased for higher photon energies (see Figure 1.7(d)). Anyhow, the ultra-light trapping effect close to the band gap is still visible. This behavior originates from strong parasitic back-reflections caused by higher-order flat photonic bands. However, it is still possible that other 3D photonic crystal

structures are more suitable for this application, for example, graded index ones. Up to now, 1D periodic structures such as rugate filters are found to have the highest potential [43].

1.7 Energy-Selective Structures as Intermediate Reflectors for Optical Path Enhancement in Tandem Solar Cells

The concepts described in the previous sections all aim toward maximizing the number of photons inside the absorbing region of the solar cell and thus primarily apply to single-junction solar cells. In these kind of cells every photon with an energy $E_\gamma \geq E_g$ absorbed by the absorber material with the band gap E_g initially generates an electron–hole pair of the energy E_γ, but the difference of the two energies, $E_\gamma - E_g$, is transferred as heat due to thermalization on a very short time scale ($\approx 10^{-12}$ s) [52]. Therefore, only E_g per absorbed photon is available. By the use of multiple layers of different E_g thermalization losses can be reduced. In this complex solar cell approach light trapping is needed, too, but now an additional task must be complied: Depending on their quantum energy the photons have to be distributed to the according layer. Furthermore, in case of stack-cell designs another important aspect has to be included. Stacked cells are multi-junction cells in which the active layers are electrically connected in series. Thus, the electrical current delivered by the structure is limited by the layer that generates the lowest current. Therefore, current-matching is necessary for optimum efficiency. To achieve current-matching the photon flux between the different layers has to be steered such that the generated currents are balanced.

Multi-junction cells achieve efficiencies above the single-junction limit [52, 53], while thin-film solar cells currently offer the best cost-effectiveness but at rather low efficiency. The micromorph tandem solar cell has the potential to combine the advantages of both cell concepts [54]. A micromorph tandem solar cell consists of a microcrystalline silicon (μc-Si) bottom cell of a few micrometer thickness and a hydrogenated amorphous silicon (a-Si:H) top cell of a thickness $< 0.3\,\mu m$ (see Figure 1.8). Ideally, the top cell ($E_g \approx 1.7$ eV) absorbs the high-energy photons while the low-energy photons are transmitted to the bottom cell ($E_g \approx 1.1$ eV). In the real world, the combined efficiency of these two layers suffers from the difference in absorbed photon flux between a-Si:H and μc-Si under AM1.5 irradiation. This leads to the above-mentioned electrical current mismatch between the two layers, which is one of the major limitations to this solar cell design.

To balance the currents and to operate the tandem solar cell at its maximum power point, intermediate reflective layers (IRLs) have been suggested [55]. These would be placed between the a-Si:H top cell and the μc-Si:H bottom cell. To tailor the photon distribution as desired, IRLs have to comply with the following criteria: High reflectance in the spectral region of low absorption of the top cell, high transmission in the spectral region of negligible absorption of the top cell, and high conductivity to avoid ohmic losses. In literature, three types of dielectric

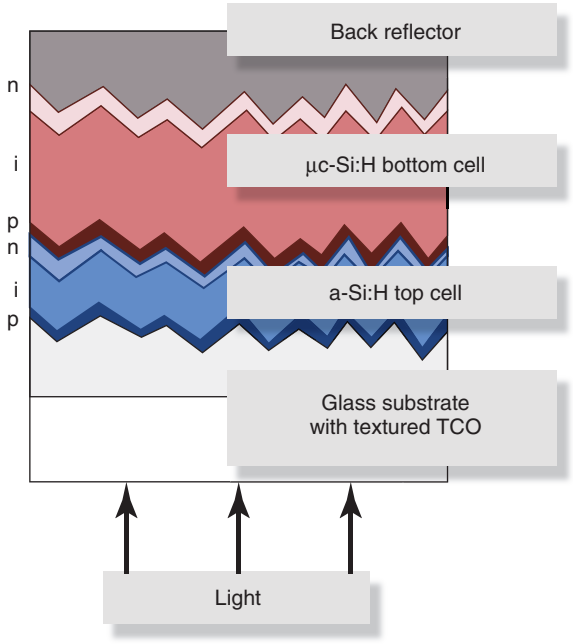

Figure 1.8 Schematic diagram of a state-of-the-art micromorph tandem solar cell without an intermediate reflector.

IRLs are predominantly discussed [56, 57]. The first type of IRL is a simple dielectric thin film that works similarly to planar interference-based ARCs as described above. They achieve a theoretical spectrally integrated absorption enhancement of $\eta_{j_{SC},theo} = 7\%$ which originates from doubling of the optical path length in the top cell [56]. The second type of IRLs are conductive Bragg reflectors, that is, is a multi-layer system that consists of two alternating conductive thin films of different refractive index. It is also based on interference but may achieve better reflectance properties than one layer only. A maximal theoretical enhancement of $\eta_{j_{SC},theo} = 20\%$ is expected [56]. 3D photonic crystal IRLs (3D-IRL) are a new class of IRL. They combine reflective and diffractive properties in a single functional layer, that is, in addition to an energy-selective redistribution an angular-selective redistribution of light is possible, which facilitates additional light-trapping mechanisms such as total internal reflection for optical path enhancement. It was shown theoretically by Bielawny *et al.* that 3D-IRLs can enhance the spectrally enhanced absorption by $\eta_{j_{SC},theo} = 28\%$ [56].

In experimental realizations of IRLs in the micromorph tandem cell ZnO or SiO_x thin-films have been successfully integrated [58–60]. However, since thin-film solar cells are commonly applied to textured substrates any advanced IRL concept, Bragg or 3D photonic crystal based, needs to be compatible with textured substrates [61]. The maximum theoretical absorption enhancements $\eta_{j_{SC},theo}$ given above are all restricted to flat substrates. Nevertheless, it was shown by Fahr

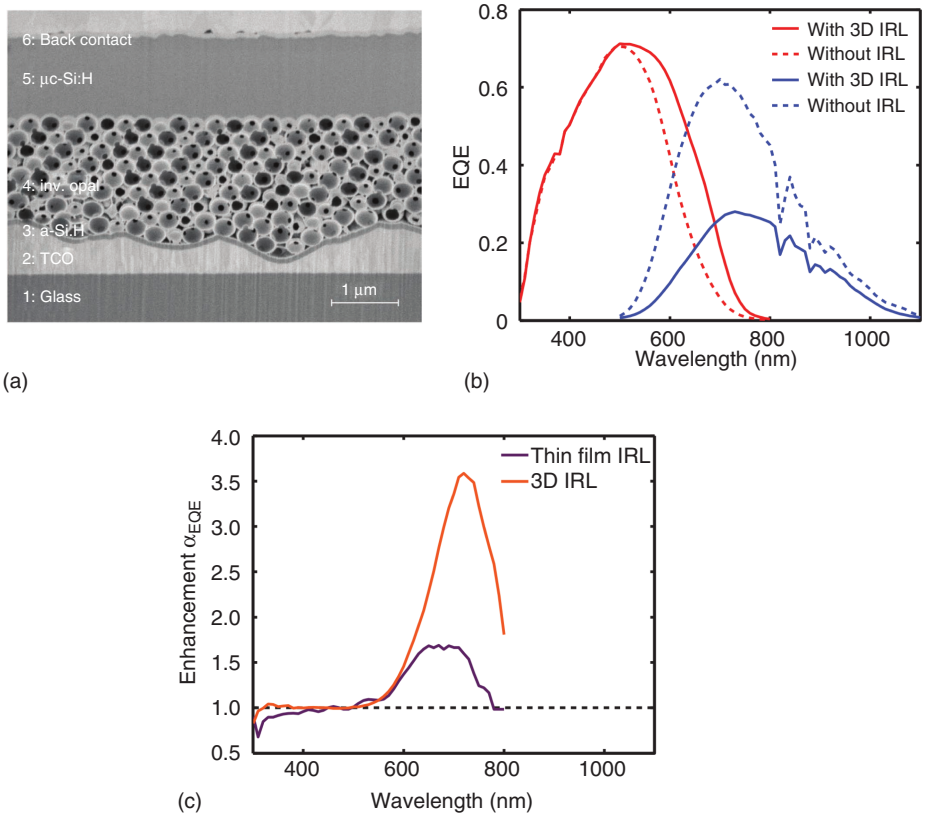

Figure 1.9 (a) Cross-sectional SEM image of the micromorph tandem cell with a 3D-photonic crystal IRL. The frontside of the cell is at the bottom. (b) Measured EQE of the micromorph tandem cell with and without a 3D-photonic crystal intermediate reflector (IRL) (red: top cell, blue:bottom cell). (c) Spectrally resolved enhancement of the EQE (α_{EQE}) of the a-Si:H top cell for a thin-film IRL (purple and for the 3D photonic crystal IRL (orange) (taken from Ref. [63]).

et al. that the given trend is still valid for textured substrates [62]. A 3D-IRL on a textured substrate fully integrated into a micromorph tandem cell has been successfully realized by Üpping *et al.* [63]. Figure. 1.9 (a) shows a cross-sectional SEM image of a micromorph tandem solar cell including the 3D-IRL. Experimentally obtained EQE measurements of the a-Si:H top cell (red) and the µc-Si:H bottom cell (blue) in a tandem solar cell with (solid) and without (dashed) a 3D photonic crystal IRL are presented in Figure 1.9 (b). In the wavelength range of 500 – 800 nm the inverted opal clearly enhances the EQE of the top cell while reducing that of the bottom cell due to the redistribution of the photon flux. The short circuit current density of this top cell is $j_{SC} = 9.4$ mA cm^{-2} without IRL and $j_{SC} = 11.7$ mA cm^{-2} with the inverted opal IRL. This corresponds to an enhancement of $\eta_{jSC} = 24.5$ % which is in very good agreement with previously published numerical calculations [56]. Further simulations reveal that the maximum of the absorption of the

inverted opal is around 650 nm (not shown), which is in excellent agreement with the red shift in the absorption edge of the a-Si:H top cell (see Figure 1.9) [63].

A benchmark for the impact of the IRL is the enhancement ratio $\alpha_{EQE}(\lambda)$ that was introduced earlier. Note that α_{EQE} also displays the optical path enhancement. In Figure 1.9c experimentally determined values of $\alpha_{EQE}(\lambda)$ for a thin-film-based IRL (purple) and of our 3D photonic crystal IRL (orange) are plotted. $\alpha_{EQE}(\lambda)$ of the 3D photonic crystal IRL lies always above that of the thin-film IRL and has its maximum at about 720 nm exhibiting $\alpha_{EQE} = 3.6$ which is a factor of 2.25 larger than that of the thin-film-based IRL.

1.8 Comparison of the Concepts

The theoretical maximum path enhancements for solar (angular divergence $\Theta_S \approx 4.7$ mrad) and circumsolar (angular divergence $\Theta_C \approx 44$ mrad) irradiation, the spectral width, and the angular dependence of the light trapping concepts introduced in this chapter are summarized in Table 1.1. Generally, the light path enhancement α_{opt} of advanced light trapping concepts is increased compared to Yablonovitch-limited concepts but at the expense of spectral and/or angular acceptance. Therefore, application of these concepts to photovoltaics is highly dependent on the specific requirements and demands of the solar cell or the solar module and the area of application.

In Figure 1.10 the theoretical upper limit of the EQE enhancement α_{EQE} ($= \alpha_{opt}$) is plotted as a function of the refractive index n of the absorber material for circumsolar irradiation. It is clear from this figure that the advanced light trapping concepts presented here possess a high potential for a large α_{EQE}. Concepts based on light randomization already virtually achieve the Yablonovitch-limit experimentally, for example, by b-Si structures (see Figure 1.4(b)). The highest enhancement reported in applying a resonant light trapping scheme has been achieved by the Kimmerling group with $\alpha_{EQE} = 135$ (indicated by the red circle

Table 1.1 Overview of the different light trapping concepts for solar cells given in this book.

	Non-resonant	Resonant	Angular selective	Energy-selective
Max. path enhancement (Θ_S)	$4n^2$	$853n$	$181078n^2$	$> 2n$
Max. path enhancement (Θ_C)	$4n^2$	$91n$	$2067n^2$	$> 2n$
Spectral width	Very broad	Narrow	Broad	Broad
Angular dependence	None	Large	Very Large	Very small
Physical principle	Lambert–Beer law	Conservation of étendue	Conservation of étendue	Interference

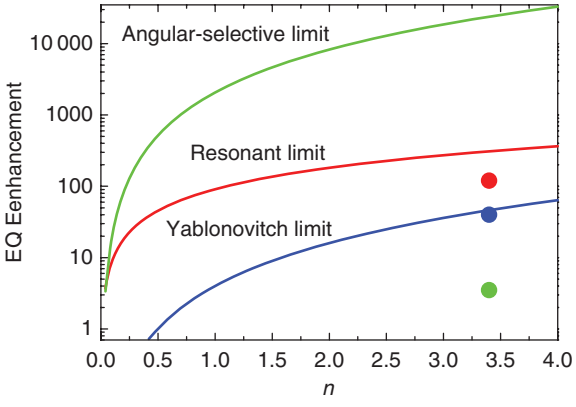

Figure 1.10 Theoretical upper limit of the integrated EQE enhancement for the Yablonovitch (blue), the resonant (red), and the angular-selective (green) light trapping concepts as a function of the refractive index *n* of the absorber material for circumsolar irradiation (Θ_C). The corresponding circles indicate the highest experimentally achieved enhancement found in literature so far [11, 38, 49].

in Figure 1.10) [38]. But still there is plenty of room to further investigate and optimize resonant light path enhancement concepts. For the experimental implementation of angular-selective structures, feasible concepts of integration into a solar cell are still lacking. Nevertheless, angular-selective light trapping structures hold the largest theoretical upper limit for enhancement and the first promising results have been achieved [49].

1.9 Conclusion

During the past 15 years, concepts to enhance the optical path length in solar cells have evolved significantly. This concerns theoretical understanding as well as experimental realization. In particular, with black silicon the Yablonovitch limit has been experimentally obtained for solar cells. More recent concepts such as resonant optical path enhancement have shown good progress in particular by the integration of photonic crystal approaches. The most demanding concept numerically as well as experimentally is probably the ultra-light trapping concepts by angular selective filters. Robust but also experimentally feasible concepts are missing. Moreover, some new ideas such as the use of slow light have just emerged, which might be of particular interest for 3D nanostructured solar cells.

References

1. ITRPV (2013) International Technology Roadmap for Photovoltaics 2013.
2. Green, M.A. (2008) Self-consistent optical parameters of intrinsic silicon at 300

K including temperature coefficients. *Sol. Energy Mater. Sol. Cells*, **92** (11), 1305–1310.
3. Campbell, P. and Green, M.A. (1987) Light trapping properties of pyramidally textured surfaces. *J. Appl. Phys.*, **62** (1), 243.
4. Campbell, P. (1993) Enhancement of light absorption from randomizing and geometric textures. *J. Opt. Soc. Am. B: Opt. Phys.*, **10** (12), 2410.
5. Zhao, J., Wang, A., Altermatt, P., and Green, M.A. (1995) Twenty-four percent efficient silicon solar cells with double layer antireflection coatings and reduced resistance loss. *Appl. Phys. Lett.*, **66** (26), 3636.
6. Chang, T.-H., Wu, P.-H., Chen, S.-H., Chan, C.-H., Lee, C.-C., Chen, C.-C., and Su, Y.-K. (2009) Efficiency enhancement in GaAs solar cells using self-assembled microspheres. *Opt. Express*, **17** (8), 6519.
7. Yablonovitch, E. (1982) Statistical ray optics. *J. Opt. Soc. Am. A*, **72** (7), 899.
8. Green, M.A. (2002) Lambertian light trapping in textured solar cells and light-emitting diodes: analytical solutions. *Prog. Photovoltaics Res. Appl.*, **10** (4), 235–241.
9. Yoo, J., Yu, G., and Yi, J. (2009) Black surface structures for crystalline silicon solar cells. *Mater. Sci. Eng., B*, **159**160, 333.
10. Koynov, S., Brandt, M.S., and Stutzmann, M. (2006) Black nonreflecting silicon surfaces for solar cells. *Appl. Phys. Lett.*, **88** (20), 203107.
11. Otto, M. *et al.* (2014) Black Silicon Photovoltaics. *Adv. Opt. Mater.* doi:10.1002/adom.201400395.
12. Li, X., Xiao, Y., Yan, C., Zhou, K., Schweizer, S.L., Sprafke, A., Lee, J.-H., and Wehrspohn, R.B. (2013) Influence of the mobility of Pt nanoparticles on the anisotropic etching properties of silicon. *ECS Solid State Lett.*, **2** (2), P22–P24.
13. Koynov, S., Brandt, M.S., and Stutzmann, M. (2007) Black multicrystalline silicon solar cells. *Phys. Status Solidi RRL*, **1** (2), R53.
14. Otto, M., Kroll, M., Käsebier, T., Salzer, R., Tünnermann, A., and Wehrspohn, R.B. (2012) Extremely low surface recombination velocities in black silicon passivated by atomic layer deposition. *Appl. Phys. Lett.*, **100** (19), 191603.
15. Gimpel, T., Höger, I., Falk, F., Schade, W., and Kontermann, S. (2012) Electron backscatter diffraction on femtosecond laser sulfur hyperdoped silicon. *Appl. Phys. Lett.*, **101** (11), 111911.
16. Stephens, R.B. and Cody, G.D. (1977) Optical reflectance and transmission of a textured surface. *Thin Solid Films*, **45**, 19–29.
17. Kroll, M., Kasebier, T., Otto, M., Salzer, R., Wehrspohn, R., Kley, E.-B., Tünnermann, A., and Pertsch, T. (2010) Optical modeling of needle like silicon surfaces produced by an ICP-RIE process. *Proc. SPIE*, **7725**, 772505.
18. Yuan, H.-C., Yost, V.E., Page, M.R., Stradins, P., Meier, D.L., and Branz, H.M. (2009) Efficient black silicon solar cell with a density-graded nanoporous surface: optical properties, performance limitations, and design rules. *Appl. Phys. Lett.*, **95** (12), 123501.
19. Fuechsel, K., Schulz, U., Kaiser, N., Kasebier, T., Kley, E.-B., and Tünnermann, A. (2010) Nanostructured SIS solar cells. SPIE Photonics for Solar Energy Systems.
20. Oh, J., Yuan, H.C., and Branz, H.M. (2012) An 18.2%-efficient black-silicon solar cell achieved through control of carrier recombination in nanostructures. *Nat. Nanotechnol.*, **7**, 1–6.
21. Repo, P., Benick, J., Vähänissi, V., Schön, J., Von Gastrowa, G., Steinhauser, B., Schubert, M.C., and Hermle, M. (2013) n-type black silicon solar cells. *Energy Procedia*, **38**, 866–871.
22. Ziegler, J., Otto, M., Sprafke, A.N., and Wehrspohn, R.B. (2013) Activation of Al_2O_3 passivation layers on silicon by microwave annealing. *Appl. Phys. A*, **113** (2), 285–290.
23. Song, J.-W., Jung, J.-Y., Um, H.-D., Li, X., Park, M.-J., Nam, Y.-H., Shin, S.-M., Park, T.J., Wehrspohn, R.B., and Lee, J.-H. (2014) Degradation mechanism of Al_2O_3 passivation in nanostructured Si solar cells. *Adv. Mater. Interfaces*, **1** (5), 1400010. doi: 10.1002/admi.201400010.

24. Wehrspohn, R., Sprakfe, A., Gombert, A., and Rau, U. (eds) (2015) *Photon-management in Solar Cells*, Wiley-VCH Verlag GmbH.
25. Petit, R. (ed.) (1980) *Electromagnetic Theory of Gratings*, Springer-Verlag.
26. Rayleigh, L. (1907) Note on the remarkable case of diffraction spectra described by Prof. Wood. *Philos. Mag.*, **14** (79), 60.
27. Peters, M., Bielawny, A., Bläsi, B., Carius, R., Glunz, S.W., Goldschmidt, J.C., Hauser, H., Hermle, M., Kirchartz, T., Löper, P., Üpping, J., Wehrspohn, R.B., and Willeke, G. (2010) Photonic concepts for solar cells, in *Physics of Nanostructured Solar Cells* (eds V. Badescu and M. Paulescu), NOVA Science Publishers, Inc.
28. Yee, K. (1966) Numerical solution of initial boundary value problems involving maxwell's equations in isotropic media. *IEEE Trans. Antennas Propag.*, **14** (3), 302.
29. Yu, Z., Raman, A., and Fan, S. (2010) Fundamental limit of nanophotonic light trapping in solar cells. *Proc. Natl. Acad. Sci. U.S.A.*, **107** (41), 17491.
30. Gale, M.T., Curtis, B., Kiess, H.G., and Morf, R.H. (1990) Design and fabrication of submicron grating structures for light trapping in silicon solar cells. *Proc. SPIE*, **1272**, 60–66.
31. Heine, C. and Morf, R.H. (1995) Submicrometer gratings for solar energy applications. *Appl. Opt.*, **34** (14), 2476.
32. Bermel, P., Luo, C., Zeng, L., Kimerling, L.C., and Joannopoulos, J.D. (2007) Improving thin-film crystalline silicon solar cell efficiencies with photonic crystals. *Opt. Express*, **15** (25), 16986.
33. Ferry, V.E., Munday, J.N., and Atwater, H. (2010) Design considerations for plasmonic photovoltaics. *Adv. Mater.*, **22** (43), 4794.
34. Atwater, H. and Polman, A. (2010) Plasmonics for improved photovoltaic devices. *Nat. Mater.*, **9** (3), 205.
35. Zaidi, S.H., Gee, J.M., and Ruby, D.S. (2000) Diffraction grating structures in solar cells. IEEE Photovoltaic Specialists Conference, p. 395.
36. Stiebig, H., Haase, C., Zahren, C., Rech, B., and Senoussaoui, N. (2006) Thin-film silicon solar cells with grating couplers–an experimental and numerical study. *J. Non-Cryst. Solids*, **352** (920), 1949.
37. Michel, J. and Kimerling, L.C. (2007) Design of highly efficient light-trapping structures for thin-film crystalline silicon solar cells. *IEEE Trans. Electron Devices*, **54** (8), 1926.
38. Zeng, L., Yi, Y., Hong, C., Liu, J., Feng, N., Duan, X., Kimerling, L.C., and Alamariu, Ba. (2006) Efficiency enhancement in Si solar cells by textured photonic crystal back reflector. *Appl. Phys. Lett.*, **89** (11), 111111.
39. Varghese, L.T., Xuan, Y., Niu, B., Fan, L., Bermel, P., and Qi, M. (2013) Enhanced photon management of thin-film silicon solar cells using inverse opal photonic crystals with 3D photonic bandgaps. *Adv. Opt. Mater.*, **1** (10), 692–698.
40. Chutinan, A. and John, S. (2008) Light trapping and absorption optimization in certain thin-film photonic crystal architectures. *Phys. Rev. A*, **78** (2), 1.
41. Deinega, A. and John, S. (2012) Solar power conversion efficiency in modulated silicon nanowire photonic crystals solar power conversion efficiency in modulated silicon nanowire photonic crystals. *Appl. Phys. Lett.*, **112**, 074327.
42. Gomard, G., Meng, X., Drouard, E., El Hajjam, K., Gerelli, E., Peretti, R., Fave, A., Orobtchouk, R., Lemiti, M., and Seassal, C. (2012) Light harvesting by planar photonic crystals in solar cells: the case of amorphous silicon. *J. Opt.*, **14** (2), 024011.
43. Ulbrich, C., Fahr, S., Üpping, J., Peters, M., Kirchartz, T., Rockstuhl, C., Wehrspohn, R., Gombert, A., Lederer, F., and Rau, U. (2008) Directional selectivity and ultra-light-trapping in solar cells. *Phys. Status Solidi A*, **205** (12), 2831.
44. Goetzberger, A. (1981) Optical confinement in thin Si-solar cells by diffuse back reflectors. IEEE Photovoltaic Specialists Conference, p. 867.
45. Minano, J.C. (1990) Optical confinement in photovoltaics, in *Physical Limitations to the Photovoltaic Solar Energy Conversion* (eds A. Luque and G.L. Araujo), Hilger, Bristol.
46. Shockley, W. and Queisser, H.J. (1961) Detailed balance limit of efficiency of

p-n junction solar cells. *J. Appl. Phys.*, **32** (3), 510.
47. Araujo, G. and Marti, A. (1994) Absolute limiting efficiencies for photovoltaic energy conversion. *Sol. Energy Mater. Sol. Cells*, **33**, 213.
48. Höhn, O., Kraus, T., Bauhuis, G., Schwarz, U.T., and Bläsi, B. (2014) Maximal power output by solar cells with angular confinement. *Opt. Express*, **22** (S3), A715.
49. Ulbrich, C., Peters, M., Bläsi, B., Kirchartz, T., Gerber, A., and Rau, U. (2010) Enhanced light trapping in thin-film solar cells by a directionally selective filter. *Opt. Express*, **18** (S2), A133.
50. Bovard, B.G. (1993) Rugate filter theory: an overview. *Appl. Opt.*, **32** (28), 5427.
51. Fahr, S., Ulbrich, C., Kirchartz, T., Rau, U., Rockstuhl, C., and Lederer, F. (2008) Rugate filter for light-trapping in solar cells. *Opt. Express*, **16** (13), 9332.
52. Würfel, P. (2005) *Physics of Solar Cells*, Wiley-VCH Verlag GmbH.
53. Conibeer, G. and Green, M.A. (2003) Third-generation photovoltaics. *Mater. Today*, **10** (11), 42–50.
54. Fischer, D., Dubail, S., Vaucher, N.P., Kroll, U., Tomes, P., Keppner, H., Wyrsch, N., and Shah, A. (1996) The "micromorph" solar cell: extending a-Si:H technology towards thin film crystalline silicon. IEEE Photovoltaic Specialists Conference, p. 1053.
55. Yamamoto, K., Yoshimi, M., Tawada, Y., Fukuda, S., Sawada, T., Meguro, T., Takata, H., Suezaki, T., Koi, Y., Hayashi, K., Suzuki, T., Ichikawa, M., and Nakajima, A. (2002) Large area thin film Si module. *Sol. Energy Mater. Sol. Cells*, **74**, 449.
56. Bielawny, A., Rockstuhl, C., Lederer, F., and Wehrspohn, R.B. (2009) Intermediate reflectors for enhanced top cell performance in photovoltaic thin-film tandem cells. *Opt. Express*, **17** (10), 8439.
57. O'Brien, P.G., Chutinan, A., Leong, K., Kherani, N.P., Ozin, G.A., and Zukotynski, S. (2010) Photonic crystal intermediate reflectors for micromorph solar cells: a comparative study. *Appl. Phys. Lett.*, **18** (5), 4478.
58. Buehlmann, P., Bailat, J., Domine, D., Billet, A., Meillaud, F., Feltrin, A., and Ballif, C. (2007) In situ silicon oxide based intermediate reflector for thin-film silicon micromorph solar cells. *Appl. Phys. Lett.*, **91** (14), 143505.
59. Das, C., Lambertz, A., Huepkes, J., Reetz, W., and Finger, F. (2008) A constructive combination of antireflection and intermediate-reflector layers for a-Si-µc-Si thin film solar cells. *Appl. Phys. Lett.*, **92** (5), 053509.
60. Soederstroem, T., Haug, F.-J., Niquille, X., Terrazzoni, V., and Ballif, C. (2009) Asymmetric intermediate reflector for tandem micromorph thin film silicon solar cells. *Appl. Phys. Lett.*, **94** (6), 063501.
61. Bielawny, A., Üpping, J., Miclea, P.T., Wehrspohn, R.B., Rockstuhl, C., Lederer, F., Peters, M., Steidl, L., Zentel, R., Lee, S.-M., Knez, M., Lambertz, A., and Carius, R. (2008) 3D photonic crystal intermediate reflector for micromorph thin-film tandem solar cell. *Phys. Status Solidi A*, **205** (12), 2796.
62. Fahr, S., Rockstuhl, C., and Lederer, F. (2010) The interplay of intermediate reflectors and randomly textured surfaces in tandem solar cells. *Appl. Phys. Lett.*, **97** (17), 173510.
63. Üpping, J., Bielawny, A., Wehrspohn, R.B., Beckers, T., Carius, R., Rau, U., Fahr, S., Rockstuhl, C., Lederer, F., Kroll, M., Pertsch, T., Steidl, L., and Zentel, R. (2011) Three-dimensional photonic crystal intermediate reflectors for enhanced light-trapping in tandem solar cells. *Adv. Mater.*, **23** (34), 3896.